

<https://www.overleaf.com/project/63e8fa7b858beec75fd8fdc>

DRAFT VERSION MARCH 14, 2024

Typeset using L^AT_EX **manuscript** style in AASTeX631

Limits on the OH Molecule in the Smith High Velocity Cloud

ANTHONY H. MINTER,¹ FELIX J. LOCKMAN,¹ S. A. BALASHEV,² AND H. ALYSON FORD³

¹*Green Bank Observatory, Green Bank, WV 24944, USA*

²*Independent Researcher*

³*Steward Observatory and Department of Astronomy, University of Arizona, 933 N. Cherry Ave., Tucson, AZ 85721*

ABSTRACT

We have used the Green Bank Telescope (GBT) to search for the OH molecule at several locations in the Smith Cloud, one of the most prominent of the high-velocity clouds that surround the Milky Way. Five positions with a high HI column density were selected as targets for individual pointings, along with a square degree around a molecular cloud detected with the Planck telescope near the tip of the Smith Cloud. Gas in the Galactic disk with similar values of N_{HI} has detectable OH emission. Although we found OH at velocities consistent with the foreground Aquila molecular cloud, nothing was found at the velocity of the Smith Cloud to an rms level of 0.7 mK (T_b) in a 1 km s^{-1} channel. **The three positions that give the strictest limits on OH are analyzed in detail. Their combined data** imply a 5σ limit on $N(\text{H}_2)/N_{\text{HI}} \leq 0.03$ scaled by a factor dependent on the OH excitation temperature and background continuum $T_{\text{ex}}/(T_{\text{ex}} - T_{\text{bg}})$. There is no evidence for far-infrared emission from dust within the Smith Cloud. These results are consistent with expectations for a low-metallicity diffuse

Corresponding author: A.H. Minter

tminter@nrao.edu

arXiv:2403.08704v1 [astro-ph.GA] 13 Mar 2024

cloud exposed to the radiation field of the Galactic halo **rather than a product of a galactic fountain.**

Keywords: ISM: clouds – ISM: individual objects (Smith Cloud) – ISM: molecules –
ISM:dust

1. INTRODUCTION

The Smith Cloud is one of the most prominent Galactic high-velocity clouds (Smith 1963). It extends over more than 10° on the sky in neutral hydrogen emission with a highly-organized cometary morphology. It contains at least $10^6 M_\odot$ of HI and probably an equal mass in ionized gas but no obvious stellar component (Lockman et al. (2008) hereafter L08; Hill et al. (2009); Stark et al. (2015)). Its metallicity is about one-half solar with an average $[Z] = -0.28 \pm 0.14$, and it is draped in a magnetic field (Hill et al. 2009; Fox et al. 2016; Betti et al. 2019).

There are several proposals for the origin of the Smith Cloud. It could be the tidal remnant of an accreting dwarf galaxy; the baryonic component of a dark matter sub-halo; the product of a galactic fountain driven by multiple supernovae in the Milk Way disk (Bland-Hawthorn et al. 1998; Nichols & Bland-Hawthorn 2009; Nichols et al. 2014; Galyardt & Shelton 2016; Marasco & Fraternali 2017). If the Smith Cloud is indeed a tidal remnant, or is the product of a Galactic fountain, it may contain a molecular phase in addition to its HI and H^+ .

At the $9.1'$ angular resolution of the GBT the 21cm neutral hydrogen emission from the Smith Cloud reaches a maximum brightness temperature $T_b \approx 15$ K, and a maximum column density $N_{\text{HI}} \approx 6 \times 10^{20} \text{ cm}^{-2}$. This value of N_{HI} is several times greater than the atomic-to-molecular transition observed at high Galactic latitudes (Gillmon et al. 2006) and is comparable to high-latitude Galactic sightlines that have a molecular hydrogen fraction $\gtrsim 10\%$ (Liszt & Gerin 2023; Shull & Panopoulou 2024). Diffuse interstellar clouds, and even some intermediate velocity clouds at this HI column density have a molecular component that is detectable in the 18 cm radio lines of OH (Barriault et al. 2010; Smith et al. 2018; Tang et al. 2021). Moreover, in a study of a sightlines through the outer Milky Way, Busch et al. (2021) detect OH emission in the 1667 MHz line at intensities $T_b(1667) \gtrsim 4$

mK at all velocities where the HI emission is $T_b(21\text{cm}) \gtrsim 10$ K, an HI brightness temperature in the range of that seen in the Smith Cloud.

Because the relative abundance ratios OH/HI, and OH/H₂ are sensitive to physical conditions in diffuse interstellar gas (e.g., [Balashev et al. 2021](#)), we used the GBT to search for emission from the 18cm transitions of OH at five positions in the Cloud. In addition, we searched for OH over a 1 sq-degree field at the tip of the Cloud, where there is evidence of CO emission from the Planck survey ([Planck Collaboration et al. 2014](#)), **though that survey detects only total CO and cannot distinguish kinematically between foreground gas and the Smith Cloud.** Three directions where $T_B(\text{HI}) > 14$ K and $N_{\text{HI}} \geq 4.5 \times 10^{20}$ cm⁻² were observed to a sensitivity level sufficient to detect the 1667 MHz line from an equivalent Galactic interstellar cloud, or from the interstellar gas detected in OH by [Busch et al. \(2021\)](#) on long paths through the outer Galactic disk. Although we will focus on the data from these three directions as they give the most sensitive limits on OH in the Smith Cloud, our conclusions apply to the other fields as well but with less strict limits.

[Tang et al. \(2021\)](#) give a recent summary of expectations for OH emission. There are four 18 cm transitions of **ground state** OH, two main lines at 1665 and 1667 MHz, and satellite lines at 1612 and 1720 MHz. In Local Thermodynamic Equilibrium (LTE) the 1665 and 1667 MHz lines should be 5 and 9 times brighter than the satellite lines, respectively. Local effects arising from the intensity of the infrared radiation field commonly cause deviations from the expected line ratios. It is not clear what to expect for OH excitation conditions in the Smith Cloud, as it lies in the lower halo where local sources of infrared radiation should be rare, but where the Cloud is impacted by diffuse ionizing radiation escaping from the Galactic disk ([Bland-Hawthorn et al. 1998](#); [Bland-Hawthorn & Maloney 2002](#); [Putman et al. 2003](#); [Fox et al. 2016](#)).

For this paper we adopt the basic properties of the Smith Cloud from L08: the densest parts of the Cloud are 12.4 ± 1.3 kpc from the Sun, at $z = -2.9 \pm 0.3$ kpc from the Galactic plane; its extent in HI is > 3 kpc. The Cloud lies toward the inner galaxy only $\approx 15^\circ$ from the Galactic plane and is viewed through a significant foreground of unrelated gas and dust.

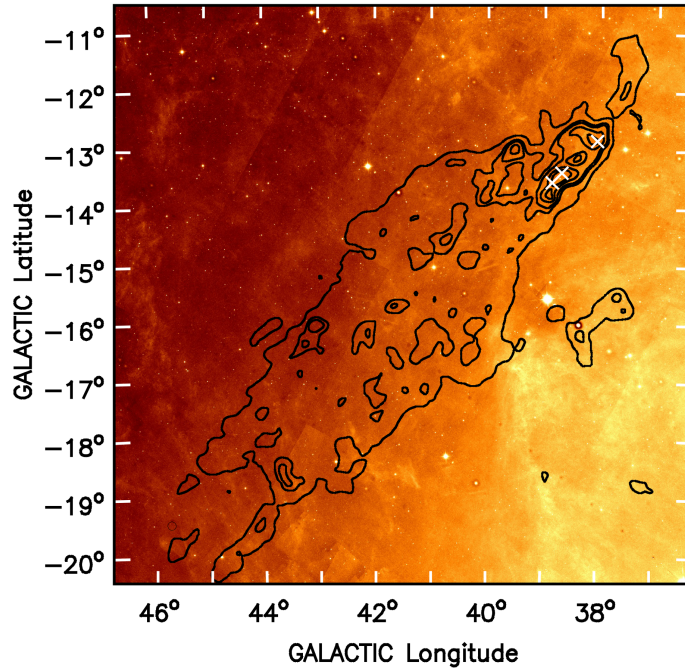


Figure 1. HI column density in contours plotted atop WISE $22\mu\text{m}$ image that shows emission from the dust along the line of sight. White crosses show the locations of the individual OH pointings described in Tables 2 and 3. HI contours are drawn at $0.5, 1.4, 1.8, 2.9,$ and $3.8 \times 10^{20} \text{ cm}^{-2}$. The WISE $22 \mu\text{m}$ image has arbitrary units as obtained from NASA’s HEASARC SkyView.

In Section 2 we describe the observations of HI and OH. Section 3 describes the conversion of the observations into limits on $N(\text{OH})$ and related quantities. The question of dust in the Smith Cloud is examined in Section 4. The implications of these results on models for the Smith Cloud are discussed in Section 5, and Section 6 gives a brief summary.

2. OBSERVATIONS

Observations of the 18 cm lines of OH and the 21cm line of HI were made with the GBT (Prestage et al. 2009) using the L band receiver and the VEGAS spectrometer. The GBT has an angular resolution of $7.5'$ and $9.1'$ at the frequencies of the OH and HI lines, respectively, **and the main beam efficiency is 0.83 for both species. Observational parameters are summarized in Table 1, where V_{LSR} is the velocity range covered, and δv is the channel spacing. Col. 6 gives the typical rms noise in a channel and col. 5 the typical integration time spent at each of the three most important positions.**

Table 1. GBT Observational Summary

Species	HPBW	V_{LSR} range	δv	t_{int}^a	σT_b^a
	(')	(km s^{-1})	(km s^{-1})	(min)	(mK)
(1)	(2)	(3)	(4)	(5)	(6)
HI	9.1	± 400	1.03	0.3	67
OH	7.5	$-585 \rightarrow +800$	1.10	2700	0.7

^aTypical values

2.1. HI Observations

For this work we use 21cm HI observations from the GBT made as part of a new survey of the Smith Cloud. These data have improvements in calibration, velocity coverage, and velocity resolution compared to the data presented in L08. Data were acquired by in-band frequency switching and reduced to include all $|V_{LSR}| \lesssim 400 \text{ km s}^{-1}$ at resolution of 1.03 km s^{-1} . Spectra were calibrated, corrected for stray radiation, and converted to brightness temperature using the method described in Boothroyd et al. (2011). A low-order polynomial was fit to emission-free regions of the spectra with a resultant rms noise in brightness temperature of 67 mK in a 1 km s^{-1} channel.

The three principle positions searched for OH are marked on a WISE 22μ image along with contours of N_{HI} in Figure 1, and the measured HI spectra are given in Figure 2. The Smith Cloud HI emission is not faint; it can constitute $\gtrsim 30\%$ of the total N_{HI} in these directions.

The HI properties are summarized in Table 2, where columns 1 and 2 give the Galactic coordinates **and we divide the HI into foreground gas at $V_{LSR} < 70 \text{ km s}^{-1}$, and Smith Cloud emission which peaks around 100 km s^{-1} .** Values of N_{HI} were calculated from the usual relationships (Dickey & Lockman 1990) with an assumed HI excitation temperature (spin temperature) of 100 K. The correction for opacity increases N_{HI} by only 5% above the optically thin value. The HI lines from the Smith Cloud do not have a simple Gaussian shape. The quantity T_{pk} in col. 7 refers to the

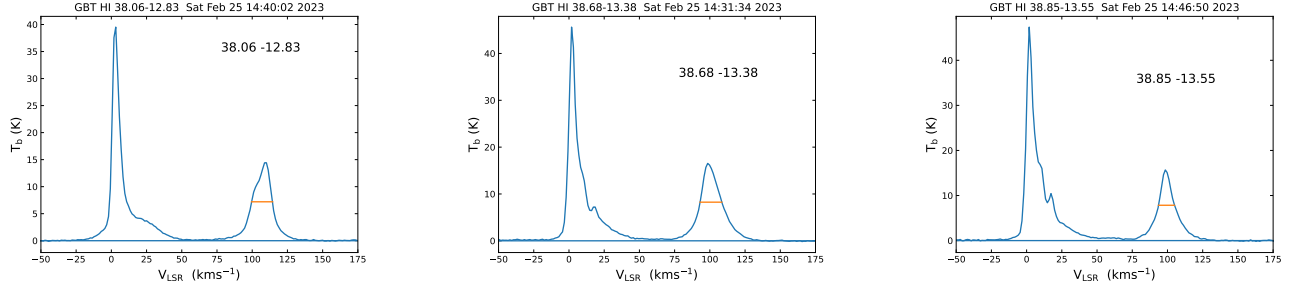


Figure 2. 21cm HI spectra toward the Smith Cloud directions that give the most strict limits on OH. The Smith Cloud emission occurs near 100 km s^{-1} ; its FWHM is indicated by a horizontal line.

Table 2. HI in Directions Searched for OH

ℓ	b	$N_{\text{HI}}(\text{for})$	$T_{\text{pk}}(\text{for})$	$V_{\text{LSR}}(\text{for})$	$N_{\text{HI}}(\text{Smith})$	$T_{\text{pk}}(\text{Smith})$	FWHM (Smith)	$V_{\text{LSR}}(\text{Smith})$	$\langle n_{\text{HI}} \rangle (\text{Smith})$
($^{\circ}$)	($^{\circ}$)	(10^{20} cm^{-2})	(K)	(km s^{-1})	(10^{20} cm^{-2})	(K)	(km s^{-1})	(km s^{-1})	(cm^{-3})
(1)	(2)	(3)	(4)	(5)	(6)	(7)	(8)	(9)	(10)
38.06	-12.83	8.2	39.5	3.0	4.6	14.4	15.0	109.0	2.3
38.68	-13.38	10.2	45.6	1.9	5.9	16.5	15.5	100.2	2.9
38.85	-13.55	11.2	47.4	1.9	4.5	15.7	11.4	99.0	2.2

NOTE— The hydrogen column density is calculated for a spin temperature of 100 K. **The 1σ uncertainty in T_{pk} is ≈ 0.07 K.** **Velocities are for the brightest line emission in the foreground (for) or Smith Cloud component.**

maximum brightness temperature in the line, and the FWHM (col. 8) is the velocity width measured at half the peak brightness.

The observed positions lie along a bright, fairly narrow ridge in the HI emission that has a FWHM ~ 0.3 . At the adopted distance of the Smith Cloud this corresponds to a transverse linear size of 65 pc. Assuming cylindrical symmetry, we use this value to convert N_{HI} to an average volume density, $\langle n_{\text{HI}} \rangle$, that is shown in col. 10 of Table 2.

2.2. OH Observations

Spectra in the four 18 cm transitions of OH were taken toward the three directions having some of the largest values of N_{HI} in the Smith Cloud, as well as a one square-degree area around the tip of the cloud. Data were acquired using in-band frequency switching. The sub-reflector was moved around the focus position by one-eighth of the 18cm wavelength to reduce the impact of standing waves in the spectra. The intrinsic velocity resolution of the OH spectra is 1.10 km s^{-1} , sufficient to resolve any expected emission. For consistency we report noise levels normalized to a 1 km s^{-1} velocity channel.

All of the OH data were flagged for undesired signals – radio frequency interference (RFI) – that appears at frequencies near the OH lines, especially the 1612 MHz line. First a derivative of each spectrum was determined by subtracting a copy of the spectrum shifted by one channel. A robust fit to the mean of the derivative was performed and points more than 5σ from the mean were identified and flagged as strong RFI. The second step involved a robust fit of a polynomial to the band-pass of each spectrum. Again, data deviating more than 5σ from the fit were flagged as RFI. The final step was to split the data into two sets by the time of observation and by polarization. As thermal main-line OH emission from interstellar clouds is not expected to vary in time or to be linearly polarized, any signal that exhibited either behavior was assumed to be spurious. This procedure identified RFI that could have otherwise been mistaken for a real signal.

No OH emission was detected that could be attributed to the Smith Cloud. The only measurable OH lines are at a low V_{LSR} and arise in the foreground Aquila molecular cloud (Dame et al. 2001). The OH observations are summarized in Table 3, which gives the rms noise limits σT_b in mK scaled to a 1 km s^{-1} channel for each position and transition (col. 6). The low-velocity emission line parameters **and their 1σ errors** were derived from a Gaussian fit (cols. 3-5). Figure 3 shows spectra in the four OH transitions averaged over the three main directions under study.

These are very sensitive OH spectra with an **rms noise $\sigma T_b \sim 0.7 \text{ mK in a } 1 \text{ km s}^{-1}$ channel in the main lines.** This is comparable to the sensitivity of the low latitudes studies of Busch et al.

Table 3. Low Velocity OH Detections

ℓ, b	Transition	T_{pk}	FWHM	V_{LSR}	σT_b	W(OH)	N_{OH}
(1)	(MHz)	(mK)	(km s ⁻¹)	(km s ⁻¹)	(mK)	(mK-km s ⁻¹)	(10 ¹³ cm ⁻²)
(1)	(2)	(3)	(4)	(5)	(6)	(7)	(8)
38.06-12.83	1612	-2 ± 1	2 ± 2	1.8 ± 0.6	0.88		
	1665	12.9 ± 0.6	2.5 ± 0.1	2.76 ± 0.06	0.67	34.4	1.4
	1667	27.4 ± 0.7	2.33 ± 0.07	2.82 ± 0.03	0.59	68.0	1.5
	1720	6.8 ± 0.6	2.5 ± 0.2	3.7 ± 0.1	0.61		
38.68-13.38	1612	-4 ± 11	1 ± 4	1.8 ± 0.2	1.04		
	1665	4.3 ± 0.7	2.9 ± 0.5	1.4 ± 0.2	0.70	13.3	0.5
	1667	11.6 ± 0.7	2.5 ± 0.2	1.62 ± 0.08	0.82	30.9	0.7
	1720	2.5 ± 0.5	4 ± 1	0.3 ± 0.5	0.64		
38.85-13.55	1612	-3 ± 1	3 ± 1	0.1 ± 0.4	1.21		
	1665	11.3 ± 0.8	2.4 ± 0.2	1.36 ± 0.08	0.67	28.9	1.2
	1667	18.5 ± 0.7	2.7 ± 0.1	1.16 ± 0.05	0.71	53.2	1.2
	1720	4.9 ± 0.6	2.4 ± 0.4	0.6 ± 0.2	0.68		

NOTE—Quantities T_{pk} , FWHM and V_{LSR} are from a Gaussian fit to the **OH lines, associated with the Aquila molecular cloud.** N_{OH} is derived from [Equation 1](#) using $\Delta T_{ex} = 1$, scaled by **9/5 for the 1665 MHz line.**

(2021). In contrast, a more typical modern OH survey, e.g., the SPLASH survey of [Dawson et al. \(2022\)](#), has a noise level ≈ 15 mK over a similar velocity interval.

3. OH IN THE SMITH CLOUD

Table 4 shows OH limits derived for the Smith Cloud. Assuming Local Thermodynamic Equilibrium (LTE), measurement of the main lines of OH can be used to place limits on the column density of the OH molecule (e.g., [Liszt & Lucas 1996](#); [Barriault et al. 2010](#)). For the 1667 MHz transition

$$N_{OH} = 2.26 \times 10^{14} \Delta T_{ex} \int T_b(1667) dv \text{ cm}^{-2} \quad (1)$$

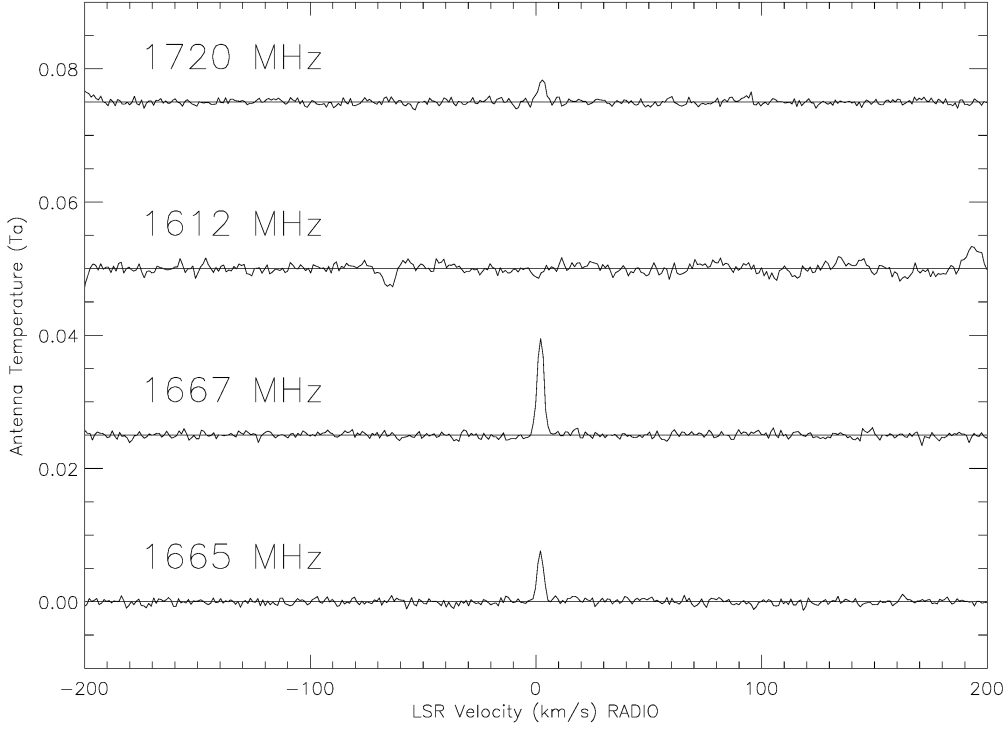


Figure 3. GBT OH spectra from the average of the three positions with the largest N_{HI} that we observed in the Smith Cloud. **Units are antenna temperature. For a spatially extended source $T_a = 0.83T_b$.** The OH lines are offset in 0.025 K increments. Any OH associated with the Smith Cloud should appear at $V_{\text{LSR}} \approx +100 \text{ km s}^{-1}$. The only OH detected is at low velocity, associated with the foreground Aquila molecular cloud.

where T_b is in Kelvins and v is in km s^{-1} (e.g., Busch et al. 2021).

The quantity ΔT_{ex} is related to the OH transition excitation temperature T_{ex} and the continuum background temperature at this frequency T_{bg} through:

$$\Delta T_{ex} = \frac{T_{ex}}{(T_{ex} - T_{bg})}. \quad (2)$$

The Smith Cloud is $\approx 3 \text{ kpc}$ from the Galactic Plane so the cosmic microwave background is likely to be the dominant component of the background continuum temperature T_{bg} . In the Galactic ISM T_{ex} can vary by an order of magnitude (e.g. Nguyen et al. (2018)) and it is not obvious what the

appropriate value of T_{ex} should be for molecules in an object as atypical as the Smith Cloud. As the Smith Cloud directions lack bright background sources, we expect that $\Delta T_{ex} \geq 1$. In the limit that $T_{ex} \gg T_{bg}$ the quantity $\Delta T_{ex} \rightarrow 1$. Barriault et al. (2010) adopted $\Delta T_{ex} = 1.0$ for the North Celestial Loop, while Busch et al. (2021) considered values $4.6 < T_{ex} < 6.1$ K and a range of T_{bg} for their analysis of OH emission on long sidelines through the outer Milky Way disk. **While it is conceivable that the excitation temperature of OH in the Smith Cloud is close to T_{bg} , allowing for a considerable abundance of OH with little emission in the 18cm lines, the fact that OH emission is detected over a range of N_{HI} in diverse environments throughout the Galaxy (e.g. Allen et al. (2012); Busch et al. (2021); Smith & Roshi (2023)), suggests that this circumstance is not common.** In the absence of any other information we consider ΔT_{ex} as an unknown, set to unity for convenient scaling.

When there is only a limit on the OH line brightness, we replace the integral in eq. 1 with the noise in a 1 km s^{-1} channel, σT_b , and sum over a velocity interval $\Delta v \text{ km s}^{-1}$. Equation 1 can then be written

$$N_{OH} \leq 7.2 \times 10^{11} \Delta T_{ex} \sqrt{\Delta v / 10} \sigma T_b \text{ cm}^{-2} \quad (3)$$

for a 1σ limit where σT_b is in mK and Δv is in km s^{-1} .

The measurements of σT_b from Table 3 are used to calculate σN_{OH} given in col. 4 of Table 4. If any molecular gas in the Smith Cloud is well-mixed with the neutral atomic hydrogen, and turbulence is small compared to thermal motions, OH emission lines should have a FWHM only 0.24 that of HI. This is unlikely to be the case as the 21cm lines are broad and often not a single Gaussian. We thus adopt $\Delta v = \text{FWHM}$ of the 21cm line from Table 1.

Table 4 gives limits on the N_{OH}/N_{HI} ratios for each observed position in the 1665 MHz and 1667 MHz transitions separately. A weighted average of the ratios for each transition is given in the row marked "Average" in Table 4. We combine limits on the two transitions assuming that the 1665 MHz and 1667 MHz lines would be in the LTE ratio of 5:9. The final average "combined" limits on

Table 4. Limits on OH in the Smith Cloud

Position	Transition	$\sigma W(\text{OH})$	σN_{OH}	$N_{\text{OH}}/N_{\text{HI}}$	$N(\text{H}_2)$	$N(\text{H}_2)/N_{\text{HI}}$
(ℓ, b)	(MHz)	(mK-km s $^{-1}$)	(10^{11}cm^{-2})	(5σ limit)	(5σ limit)	(5σ limit)
(1)	(2)	(3)	(4)	(5)	(6)	(7)
38°06 – 12°83	1665	2.6	10.6	1.1e-8	5.3e19	1.1e-1
	1667	2.3	5.2	5.6e-9	2.6e19	5.6e-2
38°68 – 13°38	1665	3.0	12.2	1.0e-8	6.1e19	1.0e-1
	1667	2.8	6.3	5.4e-9	3.2e19	5.4e-2
38°85 – 13°55	1665	2.4	9.6	1.1e-8	4.8e19	1.1e-1
	1667	2.8	6.3	7.0e-9	3.1e19	7.0e-2
Average	1665	1.5	6.1	6.2e-9	3.1e19	6.1e-2
	1667	1.5	3.4	3.4e-9	1.7e19	3.4e-2
Average	Combined		3.0	3.0e-9	1.5e19	3.0e-2

NOTE—Limits are for $\Delta T_{ex} = 1.0$. Average “combined” limits assume that the 1665 MHz and 1667 MHz transitions are in the LTE ratio.

the relative abundance of OH in the Smith Cloud are listed in the last row: $N_{\text{OH}}/N_{\text{HI}} \leq 3.0 \times 10^{-9}$ at the 5σ noise level.

Limits on the OH molecule can be used to place limits on the molecular hydrogen column density N_{H_2} through the relationship $N_{\text{OH}}/N_{\text{H}_2} = 1.0 \times 10^{-7}$ (Weselak et al. 2010; Nguyen et al. 2018; Weselak 2022) **though we note that this relationship was derived from sightlines in the Galactic disk and might not be correct for low-metallicity gas.**

The quantities in Table 4 are upper limits because no OH emission was detected at the velocity of the Smith Cloud. They are also, unfortunately, somewhat lower limits because they were derived assuming that $\Delta T_{ex} = 1$, while it is more likely that ΔT_{ex} has values of a few. Nonetheless, for plausible values of ΔT_{ex} the limits are so low that they do provide information about conditions in the Smith Cloud.

4. DUST

In the diffuse Galactic ISM there is a good correlation between dust and total gas, atomic plus molecular. This correlation can be seen in the reddening parameter $E(B-V)$ and in emission at far-infrared (FIR) wavelengths (Desert et al. 1988; Boulanger et al. 1996). A more comprehensive analysis of the dust content of the Smith Cloud will accompany the release of the new GBT HI survey; here we will discuss evidence for dust in the Smith Cloud along the sightlines searched for OH.

A recent review and analysis of a large body of data by Liszt & Gerin (2023) concludes that 1) at $N_{\text{HI}} \lesssim 10^{21} \text{ cm}^{-2}$ there is a linear relationship between N_{HI} and the reddening parameter $E(B-V)$ inferred from far infrared (FIR) emission (Schlegel et al. 1998; Gillmon et al. 2006). 2) Various investigations have found that the ratio of total proton column density to reddening, $N_{\text{H}}/E(B-V)$, is in the range $6 - 9 \times 10^{21} \text{ H nuclei cm}^{-2} \text{ mag}^{-1}$ where N_{H} includes contributions from H_2 as well as HI.

To estimate the reddening associated with the foreground gas we use the median of the values quoted in Liszt & Gerin (2023):

$$\frac{N_{\text{H}}}{E(B - V)} = (7.5 \pm 1.5) \times 10^{21} \text{ H nuclei cm}^{-2} \text{ mag}^{-1} \quad (4)$$

where the errors encompass almost the entire range of values derived by different investigations. The total N_{HI} towards the Smith Cloud can be divided into a component associated with the Smith Cloud, and foreground component that contains all HI emission except that associated with the Smith Cloud. The foreground HI component has a velocity consistent with Galactic rotation; its expected reddening is given in col. 2 of Table 5.

The Smith Cloud is observed behind low- V_{LSR} molecular gas (Table 3) that is likely associated with the Aquila molecular cloud (Dame et al. 2001), components of which are detected in CO about 10° from the tip of the Smith Cloud. The components nearest the Smith Cloud on the sky are at a distance of 400 pc, though other components may be as close as 200 pc (Su et al. 2020). The main line (1665

Table 5. Reddening E(B-V) in Directions Searched for OH

Position	HI ^a	H ₂ ^b	Total foreground ^c	FIR disk ^d	τ_{353} ^e	Difference ^f	Smith ^g
	(mag)	(mag)	(mag)	(mag)	(mag)	(mag)	(mag)
(1)	(2)	(3)	(4)	(5)	(6)	(7)	(8)
38.06–12.83	0.11 ± 0.02	$0.020\Delta T_{ex}$	0.20 ± 0.03	0.19	0.20	-0.00 ± 0.03	0.06 – 0.07
38.68–13.38	0.14 ± 0.03	$0.008\Delta T_{ex}$	0.18 ± 0.03	0.18	0.18	0.00 ± 0.03	0.08 – 0.09
38.85–13.55	0.15 ± 0.03	$0.016\Delta T_{ex}$	0.22 ± 0.03	0.24	0.24	0.02 ± 0.03	0.06 – 0.07

^aExpected reddening from foreground HI, i.e., omitting the Smith Cloud.

^bReddening from foreground molecular gas detected in low-velocity OH emission.

^cTotal foreground reddening from HI and OH for $\Delta T_{ex} = 4.5$.

^dForeground reddening from [Schlafly & Finkbeiner \(2011\)](#)

^eTotal reddening disk plus halo from FIR emission.

^fThe difference col. 6 - col. 4 that could arise in the Smith Cloud.

^gExpected reddening from the Smith Cloud if its dust emission is identical to disk gas.

MHz, 1667 MHz) OH measurements in Table 3 are used to estimate the contribution to the reddening from this foreground molecular gas using eq. 1 assuming $\Delta T_{ex} = 1$, that $N_{\text{OH}}/N_{\text{H}_2} = 1.0 \times 10^{-7}$ ([Weselak et al. 2010](#); [Nguyen et al. 2018](#); [Weselak 2022](#)), and the same relationship between N_{H} and E(B-V) as used for the HI. We combine 1667 MHz and 1665 MHz measurements of the foreground OH emission in the LTE ratio of 9:5. The results, in col. 3 of Table 5, show the explicit dependence on the quantity ΔT_{ex} .

The satellite OH lines at 1612 MHz and 1720 MHz from the foreground molecular gas show clear signs of non-LTE effects and exhibit the "conjugate pair" phenomenon, where one transition (typically the 1612 MHz) is in absorption while the conjugate transition (typically 1720 MHz) is in emission (e.g., [Petzler et al. 2020](#)). This phenomenon is the norm in the Galactic plane, with 71% of the directions in the SPLASH survey showing this pattern ([Dawson et al. 2022](#)). However, it makes these transitions not useful in estimating column densities of OH **without significant effort in radiative transfer modeling**, e.g., [Hafner et al. \(2023\)](#).

Toward the Smith Cloud the total radio continuum emission is comprised of the 2.7 K microwave background, and a non-thermal component estimated to be 1.5 K from extrapolation of the [Haslam et al. \(1981\)](#) survey in this direction. Because the Aquila molecular cloud is so close to the Sun, it is likely that the entire nonthermal component lies in the background, hence $T_{bg} = 2.7 + 1.5 = 4.2$ K. We adopt the value $T_{ex} = 5.4$ K, which is in the center of the range of T_{ex} adopted by [Busch et al. \(2021\)](#) and in the range of T_{ex} observed in Galactic molecular clouds ([Li et al. 2018](#)). This results in an excitation parameter $\Delta T_{ex} = 4.5$, which is used to scale the values in col. 3 of Table 5. When added to the reddening from foreground HI, this produces the estimated total foreground reddening given in col. 4.

An independent estimate of the foreground reddening has been made over the entire sky using far-infrared (FIR) emission calibrated by stellar reddening. Column 5 of Table 5 shows such values from [Schlafly & Finkbeiner \(2011\)](#). A measure of the total line-of-sight reddening through the Galactic disk plus halo can be derived by scaling the dust opacity at 353 GHz, $E(B - V) = 1.49 \times 10^4 \tau_{353}$, as determined from measurements by the Planck telescope ([Planck Collaboration et al. 2014, 2016](#)). This is given in col. 6. The difference between reddening associated with foreground gas and the total from the FIR is given in col. 7. *This is the reddening that is not accounted for by known foreground gas and which thus might arise in the Smith Cloud.* The values near zero indicate that the contribution of the Smith Cloud dust to τ_{353} GHz must be almost undetectable. [Shull & Panopoulou \(2024\)](#) find that Planck estimates of $E(B - V)$ in low reddening sidelines are 12% higher than the [Schlafly & Finkbeiner \(2011\)](#) values, but this is not seen toward the Smith Cloud.

The reddening expected from HI in the Smith Cloud, also derived from [Equation 4](#), is the lower value in col. 8. The larger value includes any potential reddening from the 5σ limit on N_{H_2} from Table 4. This analysis is similar to that by [Lenz et al. \(2016\)](#), [Hayakawa & Fukui \(2022\)](#), and others, and shows that all the FIR emissivity can be accounted for from foreground material. Given the expected reddening from the Smith Cloud (col. 8) it must have a dust abundance, or a FIR dust emissivity at least a factor of three lower than gas in the Galactic disk.

5. CONSTRAINTS ON THE PHYSICAL CONDITIONS

The measured column density of HI and upper limit on OH can be used to derive the constraints on the number density in the medium associated with the Smith cloud. We used the model described in [Balashev et al. 2021](#) to evaluate OH column densities. Briefly, this model calculates the abundance of OH in a diffuse cold medium by treating the analytical description of the HI/H₂ transition, ionization balance, and chemical reactions within a hydrogen and oxygen chemical network. We assume a plain parallel homogeneous cloud with number density, n_{tot} , metallicity, $[Z]$, and fixed temperature, $T = 100 \text{ K}$. This temperature value is a representative number for the cold diffuse medium, (see, e.g. [Balashev et al. 2019](#)). We note that if the cloud corresponds to the warm neutral medium with temperature $T \sim 8000 \text{ K}$, then the typical OH/HI abundance will be $\lesssim 10^{-10}$ (e.g. [Balashev et al. 2021](#)). The cloud is exposed by cosmic rays specified by primary ionization rate of hydrogen atom, ζ , in s^{-1} and by UV field denoted by χ and measured in the Mathis field units ([Mathis et al. 1983](#)) from one side. The latter mimics the situation of UV flux coming preferentially from the Milky Way. Within this model, the OH column density for a given HI column density depends on the four global physical parameters: metallicity, number density, incident UV field strength, and cosmic ray ionization rate. The observed limits on OH can constrain the combination of physical parameters.

We followed the Bayesian approach, sampling posterior distribution functions of the parameters using a Python implementation of an affine invariant Monte-Carlo Markov Chain sampler (([Goodman & Weare 2010](#)) within the *emcee* package ([Foreman-Mackey et al. 2013](#)). As was shown in [Balashev et al. \(2021\)](#), the calculated oxygen-bearing molecular abundances using this model are in agreement with the calculations using the more sophisticated code MEUDON PDR ([Le Petit et al. 2006](#)), but the significantly reduced calculation time of our code allow us to efficiently sample the physical parameter space. We considered the observational limit on the OH column density as a likelihood function, while keeping the HI column density as model parameter which sets the depth of the cloud¹. To sample the posterior probability function we used the measured HI column density as a prior,

¹ Note that OH abundance varies within the diffuse cloud, mostly due to changes of H₂ abundance (see, e.g., [Hollenbach et al. 2012](#); [Balashev et al. 2021](#)). For simplicity, we assume that UV field which defines the HI/H₂ transition falls only on one side of the cloud. We obtain almost the same results if the cloud is exposed to the same UV field from both sides.

along with Gaussian priors on the logarithm of metallicity, with mean value $[Z] = -0.28 \pm 0.14$ (Fox et al. 2016) and on the UV field. The latter was constrained to be $\log \chi = -1.2$ using a model of circumgalactic UV field by Fox et al. (2016) and the assumed distance to the Smith cloud. We took a conservative dispersion on the UV field to be 0.3 (dex), taking into account uncertainties of the distance measure and the UV flux model. For number density and ζ we assumed flat priors in log space, emulating a wide distribution.

The derived posteriors of the physical conditions for the average combined limit on the OH column density of the Smith cloud are shown in Fig. 4. One can see that we can derive an upper limit on the hydrogen number density to be $n_{\text{H}}^{\text{tot}} < 0.2 \text{ cm}^{-3}$ (1σ), which is consistent with previous estimates by Fox et al. (2016) obtained by photoionization modelling of the ions abundances detected along three sight lines towards quasars which are located at the periphery of the Smith cloud. We note that while our calculations did not consider the thermal balance, this upper limit is near the limiting value for the existence of the cold neutral phase (see e.g. Bialy & Sternberg 2019). We also derive a lower limit on the ionization parameter consistent with the Fox et al. (2016) value of $\log U > -4$. Since we calculated the H_2 abundance within the model, we also can constrain the H_2 column density at the level $\log N(\text{H}_2) < 16$ and 19 at the 2σ and 3σ confidence interval, respectively. Interestingly, the 2d posterior function shown in Fig. 4 suggests that if the number density in Smith cloud is $n \approx 0.1 \text{ cm}^{-3}$, we are close to the detection limit of OH and the H_2 column density derived from the dust (Table 5). Alternatively, if we used an estimate on the number density of $\log n_{\text{H}}^{\text{tot}} \approx -1.5$ derived by Fox et al. (2016) we should expect the H_2 column density to be $N_{\text{H}_2} \sim 10^{15} \text{ cm}^{-2}$. If we considered each sightline independently (see Table 4), we get slightly less strict upper limits on the number density, but reasonably similar limits on N_{H_2} .

6. CONCLUSIONS

The absence of OH emission from the higher N_{HI} regions of the Smith Cloud implies a fractional abundance $N_{\text{H}_2}/N_{\text{HI}} \leq 0.03\Delta T_{ex}$ at the 5σ level. This is consistent with calculations of the expected abundance in a low-metallicity diffuse cloud in the Galactic halo (Section 5).

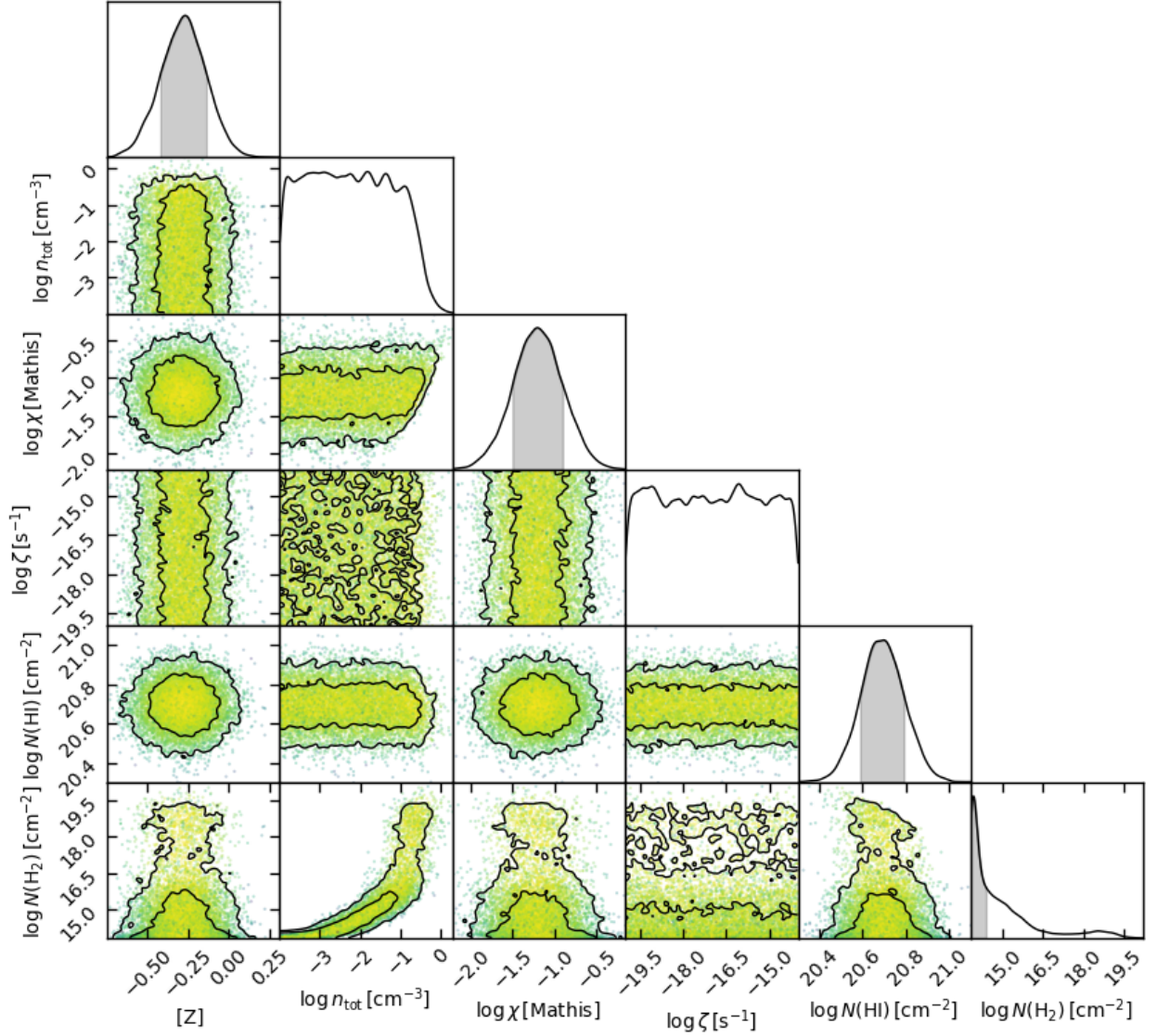


Figure 4. The 2d (off diagonal panels) and 1d (on the diagonal panels) posterior distribution function of the physical parameters and column densities obtained by MCMC sampling (Foreman-Mackey et al. 2013) of the models of OH/HI abundances. We used average N_{HI} values and upper limits on OH. The contours on the 2d posterior distribution panels correspond to the 1 and 2σ significance intervals, while the gray area marks the 1d posterior distribution corresponding to a 1σ significance interval. The 1d posterior function on the metallicity $[Z]$, UV flux (χ) and HI column density coincide with assumed priors from the measurements in this work and other studies, while the upper limits on the number density, (n_{tot}) and H_2 column density are the main result of the modelling.

Molecular gas is generally absent from HVCs except for those likely associated with the Magellanic Clouds or the Milky Way’s nuclear outflow (Putman et al. 2012; Di Teodoro et al. 2020; Cashman et al. 2021; Tchernyshyov 2022). Previous searches for evidence of FIR emission from dust in HVCs have been almost uniformly unsuccessful (e.g., Lenz et al. 2016; Shull & Panopoulou 2024, and references therein), reaching limits more than an order of magnitude lower than typical ISM values. Recently, however, Fox et al. (2023) have detected evidence of the depletion of refractory elements (Al, Fe, Si) in the HVC Complex C, indicating the presence of dust grains, though the overall metallicity of this HVC is only 0.1 - 0.3 solar (e.g., Wakker et al. 1999; Shull et al. 2011). In this regard the Smith Cloud seems typical of HVCs even though its deviation velocity, defined as the difference between its space velocity and that expected from Galactic rotation at its location, is not particularly large (Wakker & van Woerden 1991). Indeed, Smith (1963) considered it most likely that the cloud was a structure associated with the Milky Way disk. We now know that in contrast to HVCs, Intermediate Velocity Clouds have near-normal metallicities, contain molecules, and are easily detected **in OH and FIR emission (Putman et al. 2012; Lenz et al. 2015; Smith et al. 2018). In this regard IVCs resemble high-latitude diffuse molecular clouds (Magnani et al. 1996). While uncertainties in the excitation temperature of the OH transitions give the possibility that there may be large quantities of OH at undetectable levels in the Smith Cloud, when considering all the evidence we feel that the absence of significant OH emission is not misleading.** All the data on the Smith Cloud suggest that it has a low metallicity, a low dust content, a low molecular abundance, and thus a history quite different from that of Milky Way disk gas. **Further studies of the Cloud’s metallicity through UV spectroscopy of absorption line (e.g., Fox et al. (2016)) would make a major contribution our understanding of this unique object.**

7. ACKNOWLEDGMENTS

The observations were made under GBT proposal codes GBT/13B-274 and GBT/14B-513. The Green Bank Observatory is a facility of the National Science Foundation, operated under a cooperative agreement by Associated Universities, Inc. This research has made use of the NASA/IPAC

Infrared Science Archive, which is funded by the National Aeronautics and Space Administration and operated by the California Institute of Technology. This research has made use of data, software and/or web tools obtained from the High Energy Astrophysics Science Archive Research Center (HEASARC), a service of the Astrophysics Science Division at NASA/GSFC and of the Smithsonian Astrophysical Observatory's High Energy Astrophysics Division. We also used the Planck Legacy Archive and the Argonaut Skymaps. SB was supported by RSF grant 23-12-00166. We thank the anonymous referee for useful comments.

Facilities: GBT, IRSA

REFERENCES

- Allen, R. J., Ivette Rodríguez, M., Black, J. H., & Booth, R. S. 2012, *AJ*, 143, 97, doi: [10.1088/0004-6256/143/4/97](https://doi.org/10.1088/0004-6256/143/4/97)
- Balashev, S. A., Gupta, N., & Kosenko, D. N. 2021, *MNRAS*, 504, 3797, doi: [10.1093/mnras/stab1122](https://doi.org/10.1093/mnras/stab1122)
- Balashev, S. A., Klimenko, V. V., Noterdaeme, P., et al. 2019, *MNRAS*, 490, 2668, doi: [10.1093/mnras/stz2707](https://doi.org/10.1093/mnras/stz2707)
- Barriault, L., Joncas, G., Lockman, F. J., & Martin, P. G. 2010, *MNRAS*, 407, 2645, doi: [10.1111/j.1365-2966.2010.17105.x](https://doi.org/10.1111/j.1365-2966.2010.17105.x)
- Betti, S. K., Hill, A. S., Mao, S. A., et al. 2019, *ApJ*, 871, 215, doi: [10.3847/1538-4357/aaf886](https://doi.org/10.3847/1538-4357/aaf886)
- Bialy, S., & Sternberg, A. 2019, *ApJ*, 881, 160, doi: [10.3847/1538-4357/ab2fd1](https://doi.org/10.3847/1538-4357/ab2fd1)
- Bland-Hawthorn, J., & Maloney, P. R. 2002, in *Astronomical Society of the Pacific Conference Series*, Vol. 254, Extragalactic Gas at Low Redshift, ed. J. S. Mulchaey & J. T. Stocke, 267, doi: [10.48550/arXiv.astro-ph/0110044](https://doi.org/10.48550/arXiv.astro-ph/0110044)
- Bland-Hawthorn, J., Veilleux, S., Cecil, G. N., et al. 1998, *MNRAS*, 299, 611, doi: [10.1046/j.1365-8711.1998.01902.x](https://doi.org/10.1046/j.1365-8711.1998.01902.x)
- Boothroyd, A. I., Blagrove, K., Lockman, F. J., et al. 2011, *A&A*, 536, A81, doi: [10.1051/0004-6361/201117656](https://doi.org/10.1051/0004-6361/201117656)
- Boulanger, F., Abergel, A., Bernard, J. P., et al. 1996, *A&A*, 312, 256
- Busch, M. P., Engelke, P. D., Allen, R. J., & Hogg, D. E. 2021, *ApJ*, 914, 72, doi: [10.3847/1538-4357/abf832](https://doi.org/10.3847/1538-4357/abf832)
- Cashman, F. H., Fox, A. J., Savage, B. D., et al. 2021, *ApJL*, 923, L11, doi: [10.3847/2041-8213/ac3cbc](https://doi.org/10.3847/2041-8213/ac3cbc)

- Dame, T. M., Hartmann, D., & Thaddeus, P. 2001, *ApJ*, 547, 792, doi: [10.1086/318388](https://doi.org/10.1086/318388)
- Dawson, J. R., Jones, P. A., Purcell, C., et al. 2022, *MNRAS*, 512, 3345, doi: [10.1093/mnras/stac636](https://doi.org/10.1093/mnras/stac636)
- Desert, F. X., Bazell, D., & Boulanger, F. 1988, *ApJ*, 334, 815, doi: [10.1086/166879](https://doi.org/10.1086/166879)
- Di Teodoro, E. M., McClure-Griffiths, N. M., Lockman, F. J., & Armillotta, L. 2020, *Nature*, 584, 364, doi: [10.1038/s41586-020-2595-z](https://doi.org/10.1038/s41586-020-2595-z)
- Dickey, J. M., & Lockman, F. J. 1990, *ARA&A*, 28, 215, doi: [10.1146/annurev.aa.28.090190.001243](https://doi.org/10.1146/annurev.aa.28.090190.001243)
- Foreman-Mackey, D., Hogg, D. W., Lang, D., & Goodman, J. 2013, *PASP*, 125, 306, doi: [10.1086/670067](https://doi.org/10.1086/670067)
- Fox, A. J., Cashman, F. H., Kriss, G. A., et al. 2023, *ApJL*, 946, L48, doi: [10.3847/2041-8213/acc640](https://doi.org/10.3847/2041-8213/acc640)
- Fox, A. J., Lehner, N., Lockman, F. J., et al. 2016, *ApJL*, 816, L11, doi: [10.3847/2041-8205/816/1/L11](https://doi.org/10.3847/2041-8205/816/1/L11)
- Galyardt, J., & Shelton, R. L. 2016, *ApJL*, 816, L18, doi: [10.3847/2041-8205/816/1/L18](https://doi.org/10.3847/2041-8205/816/1/L18)
- Gillmon, K., Shull, J. M., Tumlinson, J., & Danforth, C. 2006, *ApJ*, 636, 891, doi: [10.1086/498053](https://doi.org/10.1086/498053)
- Goodman, J., & Weare, J. 2010, *Communications in Applied Mathematics and Computational Science*, 5, 65, doi: [10.2140/camcos.2010.5.65](https://doi.org/10.2140/camcos.2010.5.65)
- Hafner, A., Dawson, J. R., Nguyen, H., et al. 2023, *PASA*, 40, e015, doi: [10.1017/pasa.2023.8](https://doi.org/10.1017/pasa.2023.8)
- Haslam, C. G. T., Klein, U., Salter, C. J., et al. 1981, *A&A*, 100, 209
- Hayakawa, T., & Fukui, Y. 2022, arXiv e-prints, arXiv:2208.13406, doi: [10.48550/arXiv.2208.13406](https://doi.org/10.48550/arXiv.2208.13406)
- Hill, A. S., Haffner, L. M., & Reynolds, R. J. 2009, *ApJ*, 703, 1832, doi: [10.1088/0004-637X/703/2/1832](https://doi.org/10.1088/0004-637X/703/2/1832)
- Hollenbach, D., Kaufman, M. J., Neufeld, D., Wolfire, M., & Goicoechea, J. R. 2012, *ApJ*, 754, 105, doi: [10.1088/0004-637X/754/2/105](https://doi.org/10.1088/0004-637X/754/2/105)
- Le Petit, F., Nehmé, C., Le Bourlot, J., & Roueff, E. 2006, *ApJS*, 164, 506, doi: [10.1086/503252](https://doi.org/10.1086/503252)
- Lenz, D., Flöer, L., & Kerp, J. 2016, *A&A*, 586, A121, doi: [10.1051/0004-6361/201526304](https://doi.org/10.1051/0004-6361/201526304)
- Lenz, D., Kerp, J., Flöer, L., et al. 2015, *A&A*, 573, A83, doi: [10.1051/0004-6361/201424618](https://doi.org/10.1051/0004-6361/201424618)
- Li, D., Tang, N., Nguyen, H., et al. 2018, *ApJS*, 235, 1, doi: [10.3847/1538-4365/aaa762](https://doi.org/10.3847/1538-4365/aaa762)
- Liszt, H., & Gerin, M. 2023, *ApJ*, 943, 172, doi: [10.3847/1538-4357/aca83](https://doi.org/10.3847/1538-4357/aca83)
- Liszt, H., & Lucas, R. 1996, *A&A*, 314, 917
- Lockman, F. J., Benjamin, R. A., Heroux, A. J., & Langston, G. I. 2008, *ApJL*, 679, L21, doi: [10.1086/588838](https://doi.org/10.1086/588838)
- Magnani, L., Hartmann, D., & Speck, B. G. 1996, *ApJS*, 106, 447, doi: [10.1086/192344](https://doi.org/10.1086/192344)
- Marasco, A., & Fraternali, F. 2017, *MNRAS*, 464, L100, doi: [10.1093/mnrasl/slz195](https://doi.org/10.1093/mnrasl/slz195)
- Mathis, J. S., Mezger, P. G., & Panagia, N. 1983, *A&A*, 128, 212

- Nguyen, H., Dawson, J. R., Miville-Deschênes, M. A., et al. 2018, *ApJ*, 862, 49, doi: [10.3847/1538-4357/aac82b](https://doi.org/10.3847/1538-4357/aac82b)
- Nichols, M., & Bland-Hawthorn, J. 2009, *ApJ*, 707, 1642, doi: [10.1088/0004-637X/707/2/1642](https://doi.org/10.1088/0004-637X/707/2/1642)
- Nichols, M., Mirabal, N., Agertz, O., Lockman, F. J., & Bland-Hawthorn, J. 2014, *MNRAS*, 442, 2883, doi: [10.1093/mnras/stu1028](https://doi.org/10.1093/mnras/stu1028)
- Petzler, A., Dawson, J. R., & Wardle, M. 2020, *MNRAS*, 497, 4066, doi: [10.1093/mnras/staa2234](https://doi.org/10.1093/mnras/staa2234)
- Planck Collaboration, Ade, P. A. R., Aghanim, N., et al. 2014, *A&A*, 571, A13, doi: [10.1051/0004-6361/201321553](https://doi.org/10.1051/0004-6361/201321553)
- Planck Collaboration, Aghanim, N., Ashdown, M., et al. 2016, *A&A*, 596, A109, doi: [10.1051/0004-6361/201629022](https://doi.org/10.1051/0004-6361/201629022)
- Prestage, R. M., Constantikes, K. T., Hunter, T. R., et al. 2009, *IEEE Proceedings*, 97, 1382, doi: [10.1109/JPROC.2009.2015467](https://doi.org/10.1109/JPROC.2009.2015467)
- Putman, M. E., Bland-Hawthorn, J., Veilleux, S., et al. 2003, *ApJ*, 597, 948, doi: [10.1086/378555](https://doi.org/10.1086/378555)
- Putman, M. E., Peek, J. E. G., & Joungh, M. R. 2012, *ARA&A*, 50, 491, doi: [10.1146/annurev-astro-081811-125612](https://doi.org/10.1146/annurev-astro-081811-125612)
- Schlafly, E. F., & Finkbeiner, D. P. 2011, *ApJ*, 737, 103, doi: [10.1088/0004-637X/737/2/103](https://doi.org/10.1088/0004-637X/737/2/103)
- Schlegel, D. J., Finkbeiner, D. P., & Davis, M. 1998, *ApJ*, 500, 525, doi: [10.1086/305772](https://doi.org/10.1086/305772)
- Shull, J. M., & Panopoulou, G. V. 2024, *ApJ*, 961, 204, doi: [10.3847/1538-4357/ad0f20](https://doi.org/10.3847/1538-4357/ad0f20)
- Shull, J. M., Stevans, M., Danforth, C., et al. 2011, *ApJ*, 739, 105, doi: [10.1088/0004-637X/739/2/105](https://doi.org/10.1088/0004-637X/739/2/105)
- Smith, A. J., Magnani, L., Gonzalez, L., & Robishaw, T. 2018, *MNRAS*, 480, 3503, doi: [10.1093/mnras/sty1887](https://doi.org/10.1093/mnras/sty1887)
- Smith, A. J., & Roshi, D. A. 2023, *ApJ*, 948, 31, doi: [10.3847/1538-4357/acbb71](https://doi.org/10.3847/1538-4357/acbb71)
- Smith, G. P. 1963, *BAN*, 17, 203
- Stark, D. V., Baker, A. D., & Kannappan, S. J. 2015, *MNRAS*, 446, 1855, doi: [10.1093/mnras/stu2182](https://doi.org/10.1093/mnras/stu2182)
- Su, Y., Yang, J., Yan, Q.-Z., et al. 2020, *ApJ*, 893, 91, doi: [10.3847/1538-4357/ab7fff](https://doi.org/10.3847/1538-4357/ab7fff)
- Tang, N., Li, D., Yue, N., et al. 2021, *ApJS*, 252, 1, doi: [10.3847/1538-4365/abca94](https://doi.org/10.3847/1538-4365/abca94)
- Tchernyshyov, K. 2022, *ApJ*, 931, 78, doi: [10.3847/1538-4357/ac68e0](https://doi.org/10.3847/1538-4357/ac68e0)
- Wakker, B. P., & van Woerden, H. 1991, *A&A*, 250, 509
- Wakker, B. P., Howk, J. C., Savage, B. D., et al. 1999, *Nature*, 402, 388, doi: [10.1038/46498](https://doi.org/10.1038/46498)
- Weselak, T. 2022, *AcA*, 72, 233, doi: [10.32023/0001-5237/72.3.5](https://doi.org/10.32023/0001-5237/72.3.5)
- Weselak, T., Galazutdinov, G. A., Beletsky, Y., & Krelowski, J. 2010, *MNRAS*, 402, 1991, doi: [10.1111/j.1365-2966.2009.16028.x](https://doi.org/10.1111/j.1365-2966.2009.16028.x)